

Four basic symmetry types in the universal 7-cluster structure of 143 complete bacterial genomic sequences

Gorban Alexander

Centre for Mathematical Modelling, University of Leicester, UK

Popova Tatyana

Institute of Computational Modelling SB RAS, Krasnoyarsk, Russia

Zinov'yev Andrey *

Institut des Hautes tudes Scientifiques, Bures-sur-Yvette, France

February 9, 2008

Abstract

Coding information is the main source of heterogeneity (non-randomness) in the sequences of bacterial genomes. This information can be naturally modeled by analysing cluster structures in the “in-phase” triplet distributions of relatively short genomic fragments (200-400bp). We found a universal 7-cluster structure in bacterial genomic sequences and explained its properties. We show that codon usage of bacterial genomes is a multi-linear function of their genomic G+C-content with high accuracy. Based on the analysis of 143 completely sequenced bacterial genomes available in Genbank in August 2004, we show that there are four “pure” types of the 7-cluster structure observed. All 143 cluster animated 3D-scatters are collected in a database and is made available on our web-site: <http://www.ihes.fr/~zinov'yev/7clusters>. The finding can be readily introduced into any software for gene prediction, sequence alignment or bacterial genomes classification

1 Introduction

The bacterial genomes are compact genomes: most of the sequence contains coding information. Hence any statistical study of bacterial genomic sequence will detect coding information as the main source of heterogeneity (non-randomness). This is confirmed by mining sequences “from scratch”, without use of any biological information, using entropic or Hidden Markov Modeling (HMM) statistical approaches (for examples, see [1], [2], [3], [18]). All these methods can be seen as specific clustering of relatively short genomic fragments of length in the range 200-400bp comparable to the average length of a coding information piece.

Surprisingly, not much is known about the properties of the cluster structure itself, independently on the gene recognition problems, where it is implicitly used since long time ago (see, for example, early paper [5] about famous GENMARK gene-predictor, or [20] about GLIMMER approach). Only recently the structure was described explicitly. In [12], [13], [24] and [25] the structure was visualized in the 64-dimensional space of non-overlapping triplet distributions for several genomes. Also the same dataset was visualized in [14] and [11] using non-linear principal manifolds. In [19] several particular cases of this structure were observed in the context of the Z-curve methodology in the 9-dimensional space of Z-coordinates: it was claimed that the structure has interesting flower-like pattern but can be observed only for GC-rich genomes. This is somehow in contradiction with the results of [24], published before, where the same flower-like picture was demonstrated for AT-rich genome of *Helicobacter pylori*. This fact shows that this simple and basic structure is far from being completely understood and described.

The problem can be stated in the following way: there is a set of genomic fragments of length 100-1000 bp representing a genome almost uniformly. There are various ways to produce this set, for example, by sliding window with a given step of sliding (in this case sequence assembly is not generally needed), or it might be a full set of ORFs (in this case one needs to know the assembled sequence). We construct a distribution of points in a multidimensional space of statistics calculated

*To whom correspondence should be addressed: zinov'yev@ihes.fr

on the fragments and study the cluster structure of this distribution. The following questions arise: What is the number of clusters? What is the character of their mutual locations? Is there a “thin structure” in the clusters? How the structure depends on the properties of genomic sequence, can we predict it?

Every fragment can be characterized by a “frequency dictionary” of short words (see examples in [8], [9], [10], [15]). For our purposes we use frequencies of non-overlapping triplets, counted from the first basepair of a fragment. Thus every fragment is a point in 64-dimensional space of triplet frequencies. This choice is not unique, moreover, we use dimension reduction techniques to simplify this description and take the essential features. The cluster structure we are going to describe is universal in the sense that it is observed in any bacterial genome and with any type of statistics which takes into account coding phaseshifts. The structure is basic in the sense that it is revealed in the analysis in the first place, serving as the principal source of sequence non-randomness. In [12], [13], [19], [24] it was shown that even simple clustering methods like K-Means or Fuzzy K-Means give good results in application of the structure to gene-finding.

One example of the observed structure is shown on Fig.1. In short, this is a PCA plot of the point distribution. Referring for the details of the visualization to the Methods section, we stop now on basic properties of the structure. First, it consists of 7 clusters. This fact is rather natural. Indeed, we clip fragments only from the forward strand and every fragment can contain 1) piece of coding region from the forward strand, with three possible shifts relatively to the first fragment position; 2) coding information from the backward strand, with three possible frameshifts; 3) non-coding region; 4) mix of coding and non-coding information: these fragments introduce noise in our distribution, but their relative concentration is not high. Second, the structure is well pronounced, the clusters are separated from each other with visible gaps. This means that most of learning (and even self-learning) techniques aiming at separation of the clusters from each other will work very well, which is the case for bacterial gene-finders that have performance more than 90% in most cases (for recent overview, see [17]). Third, the structure is well represented by a 3D-plot (in this case it is even almost flat, i.e. 2D). Forth, it is indeed has symmetric and appealing flower-like pattern, hinting at there should be a symmetry in our statistics governing the pattern formation.

In this paper we show how the structure depends on very general properties of genomic sequence and show that it almost uniquely depends on a single parameter: the genomic G+C content. Also, based on analysis of 143 completely sequenced genomes, available in Genbank in August 2004, we describe four “pure” types of the structure observed in bacterial genomic sequences.

The outline of the paper is the following: first we introduce phaseshift and complementary reverse operators, helping to describe the structure, then we show that in nature we have almost one-dimensional set of triplet distributions. After that we explain the properties of the 7-cluster structure and describe four “pure” types of the structures, observed for bacterial genomes. The paper is finalized by the description of the methods utilized and conclusion.

2 Phaseshifts in triplet distributions

Let us denote frequencies of non-overlapping triplets for a given fragment as f_{ijk} , where $i, j, k \in \{A, C, G, T\}$, such as f_{ACT} , for example, is a relative (normalized) frequency of ACT triplet.

One can introduce such natural operations over frequency distribution as *phase shifts* $P^{(1)}, P^{(2)}$ and *complementary reversion* C^R :

$$P^{(1)} f_{ijk} \equiv \sum_{l,m,n} f_{lij} f_{kmn}, \quad P^{(2)} f_{ijk} \equiv \sum_{l,m,n} f_{lmi} f_{jkn}, \quad \hat{f}_{ijk} \equiv C^R f_{ijk} \equiv f_{\hat{k} \hat{j} \hat{i}}, \quad (1)$$

where \hat{i} is complementary to i , i.e., $\hat{A} = T, \hat{C} = G$, etc.

The phase-shift operator $P^{(n)}$ calculates a new triplet distribution, counted with a frame-shift on n positions, in the hypothesis that no correlations exist in the order of triplets in the initial phase. Complementary reversion constructs the distribution of codons from a coding region in the complementary strand, counted from the forward strand (“shadow” frequency distribution).

Phaseshift operators approximate the shifted triplet frequency as superposition of a phase-specific nucleotide frequency and a diplet frequency. This can be better understood if we rewrite definitions (1) in the following way:

$$P^{(1)} f_{ijk} \equiv \sum_l f_{lij} \sum_{m,n} f_{kmn} \equiv d_{ij}^{(right)} p_k^{(1)}, \quad P^{(2)} f_{ijk} \equiv \sum_{l,m} f_{lmi} \sum_n f_{jkn} \equiv p_i^{(3)} d_{jk}^{(left)} \quad (2)$$

We introduce the notion of *mean-field* (or *context free*) approximation of the triplet distributions in the following way:

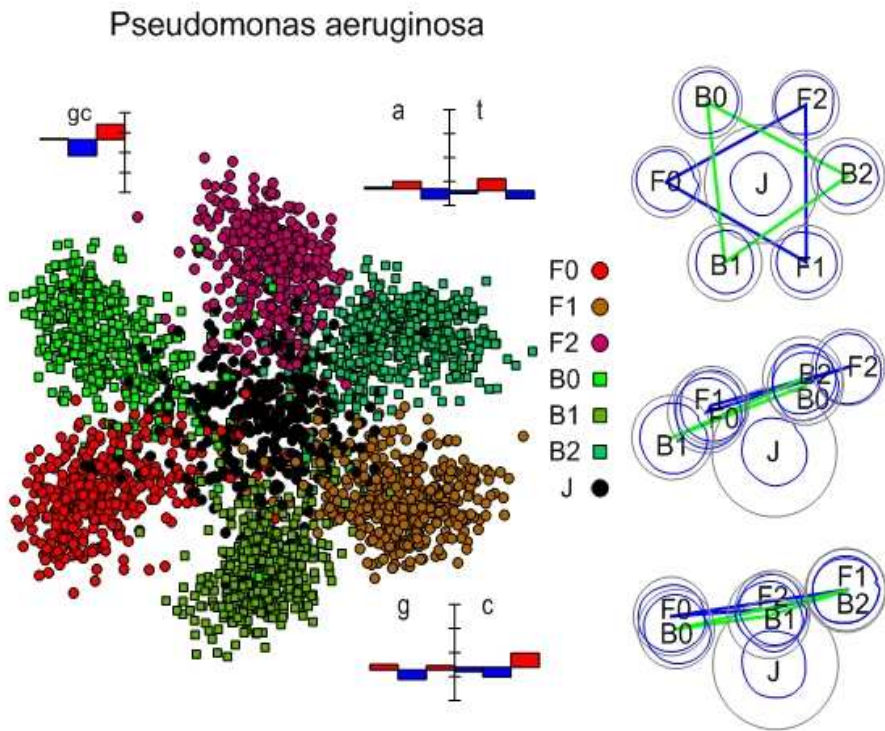


Figure 1: Seven cluster structure of *Pseudomonas aeruginosa* genomic sequence (G+C-content 67%). On the left pane the PCA plot of data distribution is shown. The colors specify a frameshift, black circles correspond to non-coding regions. On the right pane the structure is presented in a schematic way, in three projections (first and second principal components on the top, first and third in the middle, second and third in the bottom), with “radii” of the clusters schematically visualized. The diagrams show the codon position-specific nucleotide frequencies (right top and right bottom) as deviations from the average nucleotide frequency and codon position-specific G+C-content (left top).

$$m_{ijk} = p_i^{(1)} p_j^{(2)} p_k^{(3)}, \quad p_i^{(1)} = \sum_{jk} f_{ijk}, \quad p_j^{(2)} = \sum_{ik} f_{ijk}, \quad p_k^{(3)} = \sum_{ij} f_{ijk}, \quad (3)$$

i.e. the mean-field approximation is the distribution constructed from the initial triplet distribution neglecting all possible correlations in the order of nucleotides. The $p_i^{(k)}$ are the frequencies of the i th nucleotide ($i \in \{A, C, G, T\}$) at the k th position of a codon ($k = 1..3$). In this way we model the 64 frequencies of the triplet distribution using only 12 frequencies of the three position-specific nucleotide distributions. This approximation is widely used in the literature (see, for example, [3]). All triplet distributions that can be represented in the form (3) belong to a 12-dimensional curved manifold \mathbf{M} , parametrized by 12 frequencies $p_i^{(k)}$. The manifold is embedded in the 64-dimensional space of all possible triplet distributions \mathbf{T}^1 .

It is easy to understand that any phase-shift for m_{ijk} only rotates the upper (position) indexes:

$$P^{(1)} m_{ijk} = p_i^{(2)} p_j^{(3)} p_k^{(1)} = m_{kij}, \quad P^{(2)} m_{ijk} = (P^{(1)})^2 m_{ijk} = p_i^{(3)} p_j^{(1)} p_k^{(2)} = m_{jki}. \quad (4)$$

Also it is worth noticing that applying the $P^{(1)}$ (or $P^{(2)}$) operator several times to the initial triplet distribution we get the $(p_i^{(1)} p_j^{(2)} p_k^{(3)}, p_i^{(2)} p_j^{(3)} p_k^{(1)}, p_i^{(3)} p_j^{(1)} p_k^{(2)})$ triangle:

$$(P^{(1)})^3 f_{ijk} = m_{ijk}. \quad (5)$$

Operator $(P^{(1)})^3$ acts as a projector operator from full 64-dimensional distribution space \mathbf{T} onto the 12-dimensional manifold \mathbf{M} :

$$(P^{(1)})^3 : \mathbf{T} \rightarrow \mathbf{M}. \quad (6)$$

On the manifold \mathbf{M} of all possible m_{ijk} we have $P^{(2)} = (P^{(1)})^2$, therefore, there are only two operators: phaseshift $P : Pm_{ijk} = m_{jki}$ and reversion $C : Cm_{ijk} = m_{\hat{k}\hat{j}\hat{i}}$. There are following basic equalities:

$$P^3 = 1, \quad C^2 = 1, \quad PCP = C. \quad (7)$$

Let us consider a point m on \mathbf{M} . It corresponds to a set of 12 phase-specific nucleotide frequencies $p_i^{(1)}$, $p_i^{(2)}$ and $p_i^{(3)}$, $i \in \{A, C, G, T\}$. Applying operators P and C in all possible combinations we obtain an orbit on \mathbf{M} , consisting of 6 points: $m, Pm, P^2m, Cm, PCm, P^2Cm$. Theoretically, some points can coincide, but only in such a way that the resulting orbit will consist of 1 (fully degenerated case), 3 (partially degenerated case) or 6 (non-degenerated case) points. The fully degenerated case corresponds to the triplet distribution with the highest possible entropy among all distributions with the same nucleotide composition:

$$f_{ijk} = p_i p_j p_k, \quad p_i = \sum_{mn} \frac{(f_{imn} + f_{mni} + f_{nim})}{3}. \quad (8)$$

This distribution (completely random) is described by 4 nucleotide frequencies, with any information about position in the triplet lost. In our \mathbf{T} space it is a 3-dimensional (due to normalization equality) simplex on \mathbf{M} . For bacterial genomes this distribution can serve as an approximate (zero-order accuracy) model for triplet composition in non-coding regions.

Now let us consider triplet distributions corresponding to the codon usage of bacterial genomes, i.e. the subset of *naturally occurred triplet distributions*. It was found that they could be reasonably well approximated by their mean-field distributions, i.e. they are located close to \mathbf{M} . Moreover, in the next section we show that in nature, for 143 completely sequenced bacterial genomes, the m_{ijk} distributions are tightly located along one-dimensional curve on \mathbf{M} . The curve can be parametrized by the genomic G+C-content.

3 One-dimensional model of codon usage

Twelve dependencies $p_i^{(1)}(GC)$, $p_i^{(2)}(GC)$ and $p_i^{(3)}(GC)$, $i \in \{A, C, G, T\}$, where GC is genomic G+C-content, are presented on Fig.2(a-d) for 143 fully sequenced bacterial genomes available in Genbank in August, 2004. These dependencies are almost linear. This fact, despite it's simplicity, was not

¹The normalization equality $\sum_{ijk} f_{ijk} = 1$ makes all distributions to form a standard 63-dimensional simplex in R^{64} . For \mathbf{M} one has 3 independent normalizations: $\sum_i p_i^{(k)} = 1$, $k = 1..3$, these equalities distinguish a 9-dimensional set (image of the product of three 3-dimensional standard simplexes) in \mathbf{M} , where all normalized distributions are located.

explicitly demonstrated before. The numerous results on the structure of codon usage described previously in literature (see, for example, [22],[23],[21]) are in agreement with this picture.

Fig.2e demonstrates that the codon position-specific G+C-content is a linear function of genomic G+C-content, in each position. In [19] analogous results were shown for 33 completed genomes.

For our purposes, it is important to notice that for the genomes with G+C-content higher than $\sim 60\%$ there is the same well-defined structure in their codon usage: the G+C-content in the first codon position is close to the average of three values, the second is lower than the average and the third is essentially higher than the average. This pattern can be denoted in the form of simple *GC-signature*: 0 – +. In the next section we develop more complicated signature to classify 7-cluster structures, corresponding to the orbits, generated by P and C operators in a set of genomic fragments of 300-400bp length.

The linear functions, describing codon usage, are slightly different for eubacteria and archaea genomes. Significant deviations are observed for $p_A^{(1)}, p_C^{(1)}, p_G^{(3)}, p_G^{(1)}, p_T^{(3)}$ functions. For the others, the dependencies are statistically indistinguishable.

One surprising conclusion follows from Fig.2: if we take the set of triplet frequencies, occurred in nature and corresponding to the codon usage of bacterial genomes, then in the 12-dimensional space of codon position-specific nucleotide frequencies this set appears almost as a straight line (more precisely, two close lines, one for eubacteria and the other for archaea). If we look at this picture from the 64-dimensional space of triplet frequencies \mathbf{T} , then one sees that the distributions are located close to the curved \mathbf{M} manifold of the mean-field approximations, embedded in the space. As a result, when analyzing the structure of the distribution of bacterial codon usage, one detects that the points are located along two curves. These curves coincide at their AT-rich ends and diverge at GC-rich ends. Moving along these curves one meets all bacterial genomes. Genomes with close G+C-content generally have close codon usage. Many evidences for this structure were reported in studies on multivariate analysis of bacterial codon usage (for example, see Figure 6 from [16]), but here we first explain the most general structure of these representations in a clear and formal way.

4 Properties and types of the 7-cluster structure

In the paper [19] the authors claim that the codon position-specific nucleotide frequencies (represented as Z-coordinates) in GC-rich genomes show flower-like cluster structure, and the phenomenon is not observed in other genomes. Here we explain the phenomenon and demonstrate other types of structures observed in genomes and that the type of the structure is related to the pattern of symmetric properties of codon usage.

First of all, we point out to the fact that the space used in [19] is a specific projection from 64-dimensional space of triplet frequencies. The 9-dimensional phenomenon is also can be observed in 64-dimensional space and in 12-dimensional space of codon position-specific nucleotide frequencies.

Let us consider the context free approximation of codon usage introduced above:

$$m_{ijk} = p_i^{(1)} p_j^{(2)} p_k^{(3)} \quad (9)$$

and consider 3D space with the following coordinates:

$$x = p_G^{(1)} + p_C^{(1)} - f_{GC}, y = p_G^{(2)} + p_C^{(2)} - f_{GC}, z = p_G^{(3)} + p_C^{(3)} - f_{GC} \quad (10)$$

In fact, x, y and z are deviations of GC-content in the first, second and the third position from average GC-content f_{GC} of coding regions. In all GC-rich genomes (starting from $f_{GC} > 60\%$) their codon usage context-free approximation has the following structure (see Fig.2e): $x \approx 0, y < 0, z > 0$. We can denote this pattern as 0 – +. Applying phaseshift and reverse operators defined above (notice that C operator does not change G+C-content, it only reverses the signature), we obtain the following orbit: $\{0 - +, - + 0, +0 -\}$ and $\{+ - 0, -0 +, 0 + -\}$. If now we consider a 3D grid consisting of 27 nodes as shown on Fig.3, corresponding to all possible patterns (GC-signatures), then it is easy to understand that the orbit corresponds to the points of where the grid is cross-sectioned by a plane, coming through the 000 point perpendicular to the $\{---, +++\}$ diagonal. It is well known fact that in this situation the form of the intersection is a regular hexagon. The 000 point in our picture corresponds to the center of the non-coding cluster (this is the fully degenerated distribution described above), where all phases have been mixed. The $\{---, +++\}$ diagonal corresponds to the direction of the fastest G+C-content increase. Hence, this model explains the following features of the flower-like structure observed in GC-rich ($G + C > 60\%$) genomes:

- 1) In the 64-dimensional space the centers of clusters are situated close to a distinguished 2D-plane, forming regular hexagonal structure.

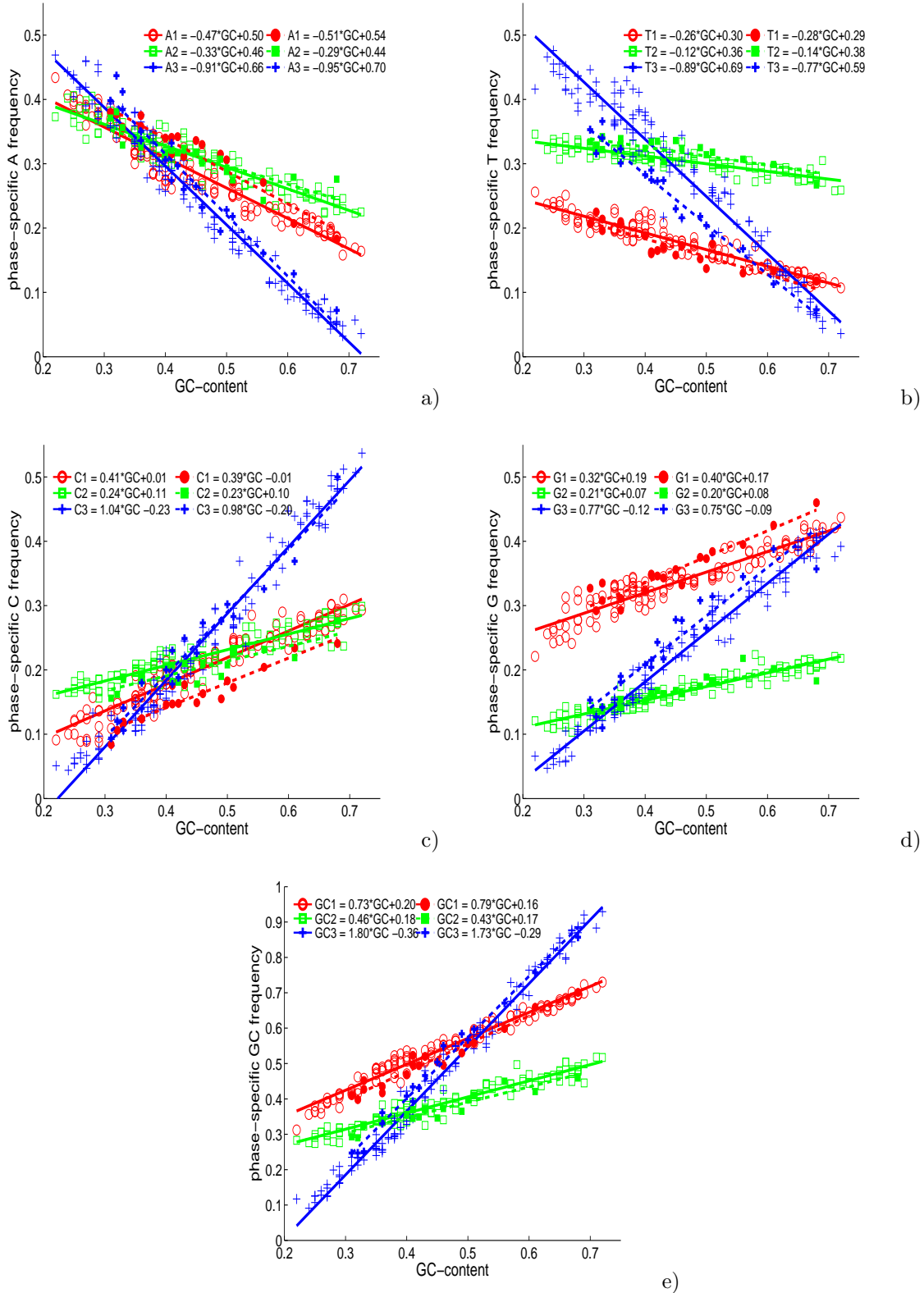


Figure 2: Codon position-specific nucleotide frequencies (a-d) and codon position-specific GC-content (e). Solid line and empty points correspond to 124 completed eubacterial genomes, broken line and filled points correspond to 19 completed archaeal genomes.

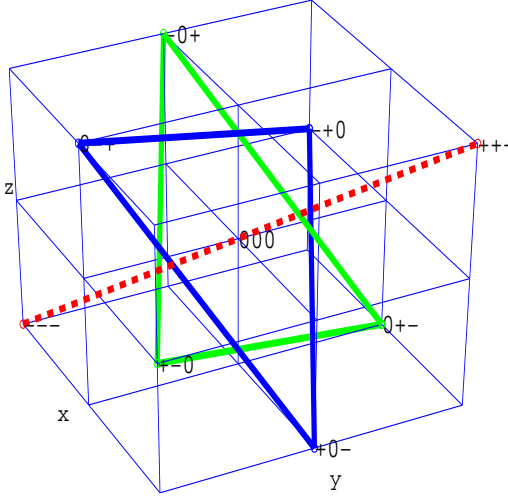


Figure 3: Model of the flower-like cluster structure. Broken line corresponds to the direction of the fastest G+C-content increase.

2) The third principal component (perpendicular to the cluster plane) is the direction of G+C-content increase (i.e., the gradient of G+C-content linear function, defined in the 64-dimensional triplet space).

In most flower-like structures the cluster that corresponds to the non-coding regions is slightly displaced in the direction perpendicular to the main cluster plane. This happens because G+C-content of non-coding regions is generally slightly lower than of coding regions.

Now let us consider general case of genome with any given genomic G+C-content. The type of the 7-cluster structure depends on values of 12 functions $p_i^{(1)}, p_i^{(2)}, p_i^{(3)}$, $i \in \{A, C, G, T\}$. Applying phaseshift and reverse operators, one obtains an orbit which serves as a skeleton of the cluster structure. The orbit structure reflects symmetries in the set of values of these 12 functions with respect to the P and C operators.

We describe these symmetries in the following simplified manner. Let us order the 12 values in the form of 6×2 table:

$$s_{ij} = \frac{p_A^{(1)} p_A^{(2)} p_A^{(3)} p_T^{(1)} p_T^{(2)} p_T^{(3)}}{p_G^{(1)} p_G^{(2)} p_G^{(3)} p_C^{(1)} p_C^{(2)} p_C^{(3)}} \quad (11)$$

Then the reverse operator C simply reads the table from right to the left:

$$Cs_{ij} = \frac{p_T^{(3)} p_T^{(2)} p_T^{(1)} p_A^{(3)} p_A^{(2)} p_A^{(1)}}{p_C^{(3)} p_C^{(2)} p_C^{(1)} p_G^{(3)} p_G^{(2)} p_G^{(1)}}. \quad (12)$$

The phaseshift operator P rotates the values in the table by threes, for every letter:

$$Ps_{ij} = \frac{p_A^{(3)} p_A^{(1)} p_A^{(2)} p_T^{(3)} p_T^{(1)} p_T^{(2)}}{p_G^{(3)} p_G^{(1)} p_G^{(2)} p_C^{(3)} p_C^{(1)} p_C^{(2)}}. \quad (13)$$

We reduce the description of s in the following way: every entry in the table is substituted by “+”, “-” and “0”, if the corresponding value is bigger then the average over the same letter frequencies, smaller or in the $[average - 0.01; average + 0.01]$ interval respectively. For example, for a set of frequencies $p_A^{(1)} = 0.3, p_A^{(2)} = 0.5, p_A^{(3)} = 0.401$, we substitute $p_A^{(1)} \rightarrow -, p_A^{(2)} \rightarrow +, p_A^{(3)} \rightarrow 0$. We call “signature” the new table \hat{s}_{ij} with reduced description.

Using linear formulas from the Fig.2(a-d) and calculating the \hat{s}_{ij} tables for the range $[0.2; 0.8]$ of G+C-content, we obtain 19 possible signatures in the intervals of genomic G+C-content, listed in Table 1.

There are 67 different signatures observed for really occurred $p_i^{(k)}$ -values for 143 genomes considered in this work (see our web-site [7] with supplementary materials). Most of them differ from the

$\begin{array}{c} \text{---} \\ \text{---} \\ \text{---} \\ \text{---} \\ \text{---} \end{array} \begin{array}{c} \text{+} \\ \text{+} \\ \text{+} \\ \text{+} \\ \text{+} \end{array} [0.200; 0.255)$	$\begin{array}{c} \text{0} \\ \text{0} \\ \text{0} \\ \text{+} \\ \text{+} \end{array} \begin{array}{c} \text{0} \\ \text{0} \\ \text{0} \\ \text{+} \\ \text{+} \end{array} [0.331; 0.373)$	$\begin{array}{c} \text{0} \\ \text{0} \\ \text{+} \\ \text{+} \\ \text{+} \end{array} \begin{array}{c} \text{+} \\ \text{+} \\ \text{+} \\ \text{+} \\ \text{+} \end{array} [0.434; 0.482)$
$\begin{array}{c} \text{---} \\ \text{---} \\ \text{---} \\ \text{---} \\ \text{---} \end{array} \begin{array}{c} \text{+} \\ \text{+} \\ \text{+} \\ \text{+} \\ \text{+} \end{array} [0.255; 0.265)$	$\begin{array}{c} \text{0} \\ \text{0} \\ \text{+} \\ \text{+} \\ \text{+} \end{array} \begin{array}{c} \text{0} \\ \text{0} \\ \text{+} \\ \text{+} \\ \text{+} \end{array} [0.373; 0.385)$	$\begin{array}{c} \text{0} \\ \text{0} \\ \text{+} \\ \text{+} \\ \text{+} \end{array} \begin{array}{c} \text{+} \\ \text{+} \\ \text{+} \\ \text{+} \\ \text{+} \end{array} [0.482; 0.487)$
$\begin{array}{c} \text{---} \\ \text{---} \\ \text{---} \\ \text{---} \\ \text{---} \end{array} \begin{array}{c} \text{+} \\ \text{+} \\ \text{+} \\ \text{+} \\ \text{+} \end{array} [0.265; 0.289)$	$\begin{array}{c} \text{0} \\ \text{0} \\ \text{+} \\ \text{+} \\ \text{+} \end{array} \begin{array}{c} \text{+} \\ \text{+} \\ \text{+} \\ \text{+} \\ \text{+} \end{array} [0.385; 0.388)$	$\begin{array}{c} \text{0} \\ \text{0} \\ \text{+} \\ \text{+} \\ \text{+} \end{array} \begin{array}{c} \text{+} \\ \text{+} \\ \text{+} \\ \text{+} \\ \text{+} \end{array} [0.487; 0.502)$
$\begin{array}{c} \text{---} \\ \text{---} \\ \text{---} \\ \text{---} \\ \text{---} \end{array} \begin{array}{c} \text{+} \\ \text{+} \\ \text{+} \\ \text{+} \\ \text{+} \end{array} [0.289; 0.316)$	$\begin{array}{c} \text{0} \\ \text{0} \\ \text{+} \\ \text{+} \\ \text{+} \end{array} \begin{array}{c} \text{+} \\ \text{+} \\ \text{+} \\ \text{+} \\ \text{+} \end{array} [0.388; 0.391)$	$\begin{array}{c} \text{0} \\ \text{0} \\ \text{+} \\ \text{+} \\ \text{+} \end{array} \begin{array}{c} \text{+} \\ \text{+} \\ \text{+} \\ \text{+} \\ \text{+} \end{array} [0.502; 0.515)$
$\begin{array}{c} \text{0} \\ \text{0} \\ \text{0} \\ \text{+} \\ \text{+} \end{array} \begin{array}{c} \text{+} \\ \text{+} \\ \text{+} \\ \text{+} \\ \text{+} \end{array} [0.316; 0.326)$	$\begin{array}{c} \text{0} \\ \text{0} \\ \text{+} \\ \text{+} \\ \text{+} \end{array} \begin{array}{c} \text{+} \\ \text{+} \\ \text{+} \\ \text{+} \\ \text{+} \end{array} [0.391; 0.424)$	$\begin{array}{c} \text{+} \\ \text{+} \\ \text{+} \\ \text{+} \\ \text{+} \end{array} \begin{array}{c} \text{+} \\ \text{+} \\ \text{+} \\ \text{+} \\ \text{+} \end{array} [0.515; 0.542)$
$\begin{array}{c} \text{0} \\ \text{0} \\ \text{0} \\ \text{+} \\ \text{+} \end{array} \begin{array}{c} \text{+} \\ \text{+} \\ \text{+} \\ \text{+} \\ \text{+} \end{array} [0.326; 0.331)$	$\begin{array}{c} \text{0} \\ \text{0} \\ \text{+} \\ \text{+} \\ \text{+} \end{array} \begin{array}{c} \text{+} \\ \text{+} \\ \text{+} \\ \text{+} \\ \text{+} \end{array} [0.424; 0.434)$	$\begin{array}{c} \text{+} \\ \text{+} \\ \text{+} \\ \text{+} \\ \text{+} \end{array} \begin{array}{c} \text{+} \\ \text{+} \\ \text{+} \\ \text{+} \\ \text{+} \end{array} [0.542; 0.545)$
		$\begin{array}{c} \text{+} \\ \text{+} \\ \text{+} \\ \text{+} \\ \text{+} \end{array} \begin{array}{c} \text{+} \\ \text{+} \\ \text{+} \\ \text{+} \\ \text{+} \end{array} [0.545; 0.800)$

Table 1: Nineteen possible signatures for one-dimensional codon usage model

signature in Table 1 with corresponding G+C value only by changing one of the “+” or “-” for “0” or vise versa.

From Table 1 one can see that the only conserved positions, independent on genomic G+C-content for the interval [0.20; 0.80] are $p_T^{(1)}$ (always “-”), $p_G^{(1)}$ (always “+”), $p_G^{(2)}$ (always “-”). This holds true also for all really observed signatures. This observation confirms already known “invariants” of codon usage described in [22],[23],[21].

Let us look at several typical examples. All genomes with genomic G+C-content higher then 60% have the following genomic signature:

$$\hat{s}_{ij}(GC > 60\%) = \begin{array}{c} \text{+} \\ \text{+} \\ \text{+} \\ \text{+} \\ \text{+} \end{array} \begin{array}{c} \text{+} \\ \text{+} \\ \text{+} \\ \text{+} \\ \text{+} \end{array} . \quad (14)$$

This signature uniformly reflects the previously mentioned GC-signature (“0-+”): pairs $p_A^{(1)}, p_T^{(1)}$ and $p_G^{(1)}, p_C^{(1)}$ compensate the signs of each other to give “0” in the first position of GC-signature, while in the second position we have “+” for A and T and “-” for G and C, and vice versa for the third position. As a result, we obtain the flower-like structure. On Fig.4 we visualize the orbit for *Streptomyces coelicolor*, genome with high G+C-content: 72%. Together with the orbit we visualize the distance matrix for the skeleton, where the distances are calculated in the full 64-dimensional triplet frequency space \mathbf{T} . Black color on the plot corresponds to zero distance, white for the biggest value in the matrix. The most informative 3×3 block of the matrix is in the left bottom corner (or top right, by symmetry): it describes mutual distances between the vertexes of two skeleton triangles. The left top and right bottom 3×3 blocks contain equal values, since the sides of the triangles have the same length.

Our second example is genome of *Fusobacterium nucleatum* (AT-rich genome, G+C-content is 27%), Fig.4b. The signature is

$$\hat{s}_{ij}(F. nucleatum) = \begin{array}{c} \text{---} \\ \text{---} \\ \text{---} \\ \text{+} \\ \text{+} \end{array} \begin{array}{c} \text{---} \\ \text{---} \\ \text{---} \\ \text{+} \\ \text{+} \end{array} . \quad (15)$$

This pattern, commonly observed in AT-rich genomes, can be called “parallel triangles”. Notice that two parallel triangles are rotated with respect to their corresponding phase labels: the F0 vertex is located in front of the B1 vertex.

The third example is genome of *Bacillus halodurans* (G+C-content is 44%):

$$\hat{s}_{ij}(B. halodurans) = \begin{array}{c} \text{---} \\ \text{---} \\ \text{---} \\ \text{+} \\ \text{+} \end{array} \begin{array}{c} \text{---} \\ \text{---} \\ \text{---} \\ \text{+} \\ \text{+} \end{array} . \quad (16)$$

We refer to this pattern as “perpendicular triangles”. Another example of the pattern is genome of *Bacillus subtilis*. All non-diagonal distances in the distance matrix have in this case approximately

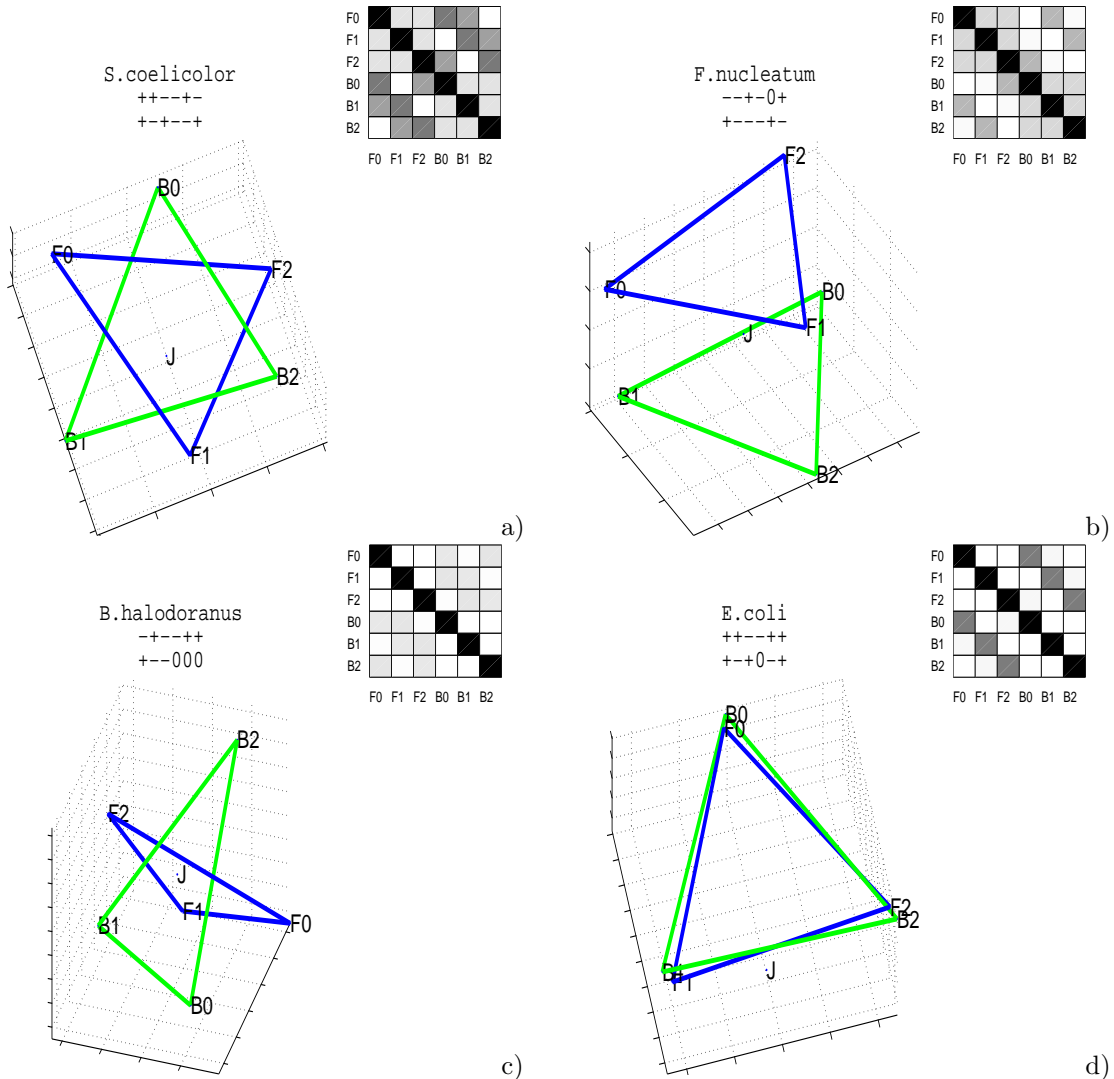


Figure 4: Four typical examples of the 7-cluster structure: a) genome of *S. coelicolor* (GC=72%), flower-like structure; b) genome of *F. nucleatum* (GC=27%), “parallel triangles”; c) *B. halodurans* (GC=44%), “perpendicular triangles”; d) *E. coli* (GC=51%), degenerated case.

the same value. This structure can be easily recognised from its signature: the second row has three zeros while the first one is almost *palindromic*. As we will see in the next example, palindromic rows in the signature (or such that can be made palindromic applying the phaseshift P operator) make zero contribution to the diagonal of the “inter-triangle” part of the distance matrix. This is easy to understand, because the reverse operator C reads the signature from right to the left. The rows with three zeros in different phase positions (when, for example, the phase specific nucleotide frequencies for one letter are equal to their average, as happened in this case) give approximately equal contribution to every value in the “inter-triangle” part of the distance matrix. The resulting matrix corresponds to the “perpendicular triangles” pattern. We should notice that the distance matrix showed on Fig.4c can not be effectively represented as a distribution of 6 points in 3D. Thus the “perpendicular triangles” structure shown on Fig.4c is only an approximate picture, the real configuration is almost 6-dimensional, due to the distance matrix symmetry.

In the region of G+C-content about 51% we observe a group of genomes with almost palindromic signatures. One typical example is the genome of *Escherichia coli*:

$$\hat{s}_{ij}(E. coli) = \begin{array}{c} + + + + \\ + - + 0 - + \end{array} . \quad (17)$$

The resulting pattern is a degenerated case: two triangles are co-located, without phase label rotation (F0 is approximately in the same point as B0). The distance matrix consists of 4 almost identical 3×3 blocks. As a result, we have situation, when 7-cluster structure effectively consists of only 4 clusters, one for every pair F0-B0, F1-B1, F2-B2 and a non-coding cluster.

The same degenerated case but with rotation of labels (F0-B1, F1-B2, F2-B0) is observed for some AT-rich genomes. For example, for the genome of *Wigglesworthia brevipalpis* (G+C-content equals 22%) the signature

$$\hat{s}_{ij}(W. brevipalpis) = \begin{array}{c} 0 - + 0 + \\ + - - + - \end{array} \quad (18)$$

becomes a perfect palindrom after applying the phaseshift operator:

$$P\hat{s}_{ij}(W. brevipalpis) = \begin{array}{c} - + 0 0 + - \\ - - + + - \end{array} . \quad (19)$$

One possible biological consequence (and even explanation) of this degeneracy is existence of overlapping genes: in this case the same codons can be used to encode proteins simultaneously in the forward and backward strands on a regular basis (without frameshift for G+C-content around 50% and with a frameshift for AT-rich genomes), with the same codon usage.

The four patterns are typical for triplet distributions of bacterial genomes observed in nature. The other ones combine features from these four “pure” types. In general, going along the G+C-content scale, we meet first “parallel triangles” which will transform gradually to “perpendicular triangles”. On this way one can even meet structures resembling flower-like type in one of the 2D-projections, like for the genome of *Helicobacter pylori* (see our web-site [7] and in [24] for the illustration). Then the pattern goes to the degenerated case with genomic G+C-content around 50% and signatures close to palindromic. After the degeneracy disappears, the pairs F0-B0, F1-B1, F2-B2 diverge in the same 2D-plane and after 55% threshold in G+C-content we almost exclusively have the flower-like structures. It is possible to browse the animated scatters of 7-cluster structures observed for every of 143 genomes on our web-site [7].

5 Web-site on cluster structures in genomic word frequency distributions

To make the images and graphs of 143 genomes 7-cluster structures available for wide public, we established a web-site [7] for cluster structures in genomic word frequency distributions.

For the moment our database contains 143 completely sequenced bacterial genomes and two types of cluster structures: the 7-cluster structure and the gene codon usage cluster structure. When browsing the database, a user can look at animated 3D-representations of these multidimensional cluster structures. For the description of the structures and the methods we refer the reader to the “intro” and “methods” pages of the web-site.

Another possibility which is provided on our web-site is browsing large-scale “maps” of various spaces where all 143 genomes can be embedded simultaneously. One example is the codon usage map: one point on the map is a genome, and close points correspond to the genomes with close codon usage. In fact, this is the same 64-dimensional triplet frequency space, used for construction of the 7-cluster

structure, “observed” from a big distance. This gives the following hierarchy of maps: general map of codon usage in 143 genomes, then the 7-cluster structure of in-phase triplet distributions, then the “thin structure” of every coding cluster: gene codon usage map. Clicking on a genome at the first map, the user “zooms” to it’s more detailed representations.

We strongly believe that the information in the database will help to advance existing tools for bacterial genomes analysis. Also it can serve as rich illustrative material for those who study sequence bioinformatics.

6 Methods

For visualization of the 7-cluster structure a data set for every 143 genome² was prepared in the following way:

1) A Genbank file with completed genome was downloaded from the Genbank FTP-site. Using BioJava package [4] the complete sequence and the annotation was parsed. In the case when the genome had two chromosomes, the sequences of both were concatenated. The short sequences of plasmids were ignored.

2) Let N be length of a given sequence S and S_i be a letter in the i th position of S . We define a step size p and a fragment size W . For given p , W and $k = 1..[\frac{N-W}{p}]$ we clip a fragment of length W in the sequence, centered in $i = w/2 + pk$. In every fragment we count frequencies of non-overlapping triplets:

$$count(c_{i_1}c_{i_2}c_{i_3}) = \sum_{i=0}^{W/3-1} comp(c_{i_1}c_{i_2}c_{i_3}, S_{i*3+1}S_{i*3+2}S_{i*3+3}), \quad (20)$$

where $comp(word1, word2)$ is a string comparison function that has value 1 if $word1$ equals $word2$ and 0 otherwise. Here c_i is a letter from genetic alphabet ($c_1 = A$, $c_2 = C$, $c_3 = G$, $c_4 = T$).

For every fragment a frequency vector is defined:

$$X_i^{c_{i_1}c_{i_2}c_{i_3}} = \frac{count(c_{i_1}c_{i_2}c_{i_3})}{\sum_{j_1,j_2,j_3} c_{j_1}c_{j_2}c_{j_3}} \quad (21)$$

All words, which contain non-standard letters like N, S, W, are ignored.

The data set X_i^j , $j = 1..[\frac{N-W}{p}]$ is normalized to have unity standard deviation and zero mean.

3) We assign to the fragment a label accordingly to the Genbank annotation of the CDS features (including hypothetical ones) that include the center of the fragment. If the center is inside a CDS feature then the reading frame and the strand of the CDS feature are determined and the fragment is assigned one of F0,F1,F2,B0,B1,B2 label. In the second case the label is J.

4) Standard PCA-analysis is performed and the first three principal components are calculated. They form a 3D-orthonormal basis in the 64-dimensional space. Every point is projected into the basis, thus we assign three coordinates for every point.

To create a schema of 7-cluster structure (see Fig.1) the following method was utilized. We calculated the mean point y^L for every subset with a given label L .

For the set of centroids $y^{F0}, y^{F1}, y^{F2}, y^{B0}, y^{B1}, y^{B2}$ a distance matrix of euclidean distances was calculated and visualized using classical MDS.

To visualize the “radii” of the subsets, a mean squared distance $d^{(p)}$ to the centroid p was calculated (intraclass dispersion). To visualize the value on 2D plane, we have to introduce dimension correction factor, so the radius drawn on the picture equals

$$r^{(p)} = \sqrt{\frac{2}{4^k}d^{(p)}} \quad (22)$$

The form of the cluster is not always spherical and often intersection of radii do not reflect real overlapping of classes in high-dimensional space. To show how good the classes are separated actually, we developed the following method for cluster contour visualization. To create a contour for class p , we calculate averages of all positive and negative projections on the vectors connecting centroid p and 6 other centroids $i = 1..6$.

$$\mathbf{n}_i^p = \frac{\mathbf{y}^i - \mathbf{y}^p}{||\mathbf{y}^i - \mathbf{y}^p||}, n_i^p(X_k) = (X_k - y^p, \mathbf{n}_i^p) \quad (23)$$

²We took only different species from GenBank, choosing the first alphabetically available strain in the list.

$$f_i^p = \frac{\sum_{n_i^p(X_k) > 0} n_i^p}{\sum_{n_i^p(X_k) > 0} 1}, b_i^p = \frac{\sum_{n_i^p(X_k) < 0} n_i^p}{\sum_{n_i^p(X_k) < 0} 1} \quad (24)$$

Then, using the 2D MDS plot where every vector $(y^p)'$ has 2 coordinates, we put 12 points t^f , t^b analogously.

$$(\mathbf{n}_i^p)' = \frac{(\mathbf{y}^i)' - (\mathbf{y}^p)'}{\|(\mathbf{y}^i)' - (\mathbf{y}^p)'\|}, \quad (25)$$

$$t_i^f = (y^i)' + f_i^p(n_i^p)', t_i^b = (y^i)' + b_i^p(n_i^p)', i = 1..6 \quad (26)$$

Using a smoothing procedure in polar coordinates we create a smooth contour approximating these 12 points.

7 Discussion

In this paper we prove the universal 7-cluster structure in triplet distributions of bacterial genomes. Some hints at this structure appeared long time ago, but only recently it was explicitly demonstrated and studied.

The 7-cluster structure is the main source of sequence heterogeneity (non-randomness) in the genomes of bacterial genomes. In this sense, our 7 clusters is the basic model of bacterial genome sequence. We demonstrated that there are four basic “pure” types of this model, observed in nature: “parallel triangles”, “perpendicular triangles”, degenerated case and the flower-like type (see Fig.4).

To explain the properties and types of the structure, which occur in natural bacterial genomic sequences, we studied 143 bacterial genomes available in Genbank in August, 2004. We showed that, surprisingly, the codon usage of the genomes can be very closely approximated by a multi-linear function of their genomic G+C-content (more precisely, by two similar functions, one for eubacterial genomes and the other one for archaea). In the 64-dimensional space of all possible triplet distributions the bacterial codon distributions are close to two curves, coinciding at their AT-rich ends and diverging at their GC-rich ends. When moving along these curves we meet all naturally occurred 7-cluster structures in the following order: “parallel triangles” for the AT-rich genomes (G+C-content is around 25%), then “perpendicular triangles” for G+C-content is around 35%, switching gradually to the degenerated case in the regions of GC=50% and, finally, the degeneracy is resolved in one plane leading to the flower-like symmetric pattern (starting from GC=60%). All these events can be illustrated using the material from the web-site we established [7].

The properties of the 7-cluster structure have natural interpretations in the language of Hidden Markov Models. Locations of clusters in multidimensional space correspond to in-state transition probabilities, the way how clusters touch each other reflects inter-state transition probabilities. Our clustering approach is independent on the Hidden Markov Modeling, though can serve as a source of information to adjust the learning parameters.

In our paper we analyzed only triplet distributions. It is easy to generalize our approach for longer (or shorter) words. In-phase hexamers, for example, are characterized by the same 7-cluster structure. However, our experience shows that the most of information is contained in triplets: the correlations in the order of codons are small and the formulas (1) work reasonably well. Other papers confirm this observation (see, for example, [1], [12]).

The subject of the paper has a lot of possible continuations. There are several basic questions: how one can explain the one-dimensional model of codon usage or why the signatures in the middle of G+C-content scale have palindromic structures? There are questions about how our model is connected with codon bias in translationally biased genomes: the corresponding cluster structure is the second hierarchical level or the “thin structure” in every cluster of the 7-cluster structure (see, for example, [6]). Also the following question is important: is it possible to detect and use the universal 7-cluster structure for higher eukaryotic genomes, where this structure also exists (see [24]), but is hidden by the huge non-coding cluster?

The information about the 7-cluster structure can be readily introduced into existing or new software for gene-prediction, sequence alignment and genome classification.

References

[1] Audic S, Claverie JM. Self-identification of protein-coding regions in microbial genomes. (1998) *Proc Natl Acad Sci USA*. **95**(17):10026-31.

- [2] Baldi P. On the convergence of a clustering algorithm for protein-coding regions in microbial genomes. (2000) *Bioinformatics*. **16**(4):367-71.
- [3] Bernaola-Galvan, P., Grosse, I., Carpenea, P., Oliver, J.L., Roman-Roldan, R., Stanley, H.E. (2000). Finding borders between coding and noncoding DNA regions by an entropic segmentation method. *Physical Review Letters* **85**(6): 1342-1345.
- [4] BioJava open-source project. <http://www.biojava.org>
- [5] Borodovsky, M., McIninch, J. (1993). GENMARK: parallel gene recognition for both DNA strands. *Comp. Chem* **17**, 123-133.
- [6] Carbone A., Zinovyev A., Kepes F. Codon Adaptation Index as a measure of dominating codon bias. (2003) *Bioinformatics*. **19**, 13, p.2005-2015.
- [7] Cluster structures in genomic word frequency distributions. Web-site with supplementary materials. <http://www.ihes.fr/~zinovyev/7clusters/index.htm>
- [8] Gorban AN, Mirkes EM, Popova TG, Sadovsky MG. A new approach to the investigations of statistical properties of genetic texts. (1993) *Biofizika* **38** (5): 762-767.
- [9] Gorban AN, Bugaenko NN, Sadovskii MG. Maximum entropy method in analysis of genetic text and measurement of its information content. (1998) *Open systems and information dynamics*. **5**, pp.265-278.
- [10] Gorban AN, Popova TG, Sadovsky MG. Classification of symbol sequences over their frequency dictionaries: towards the connection between structure and natural taxonomy. (2000) *Open System and Information Dynamics*, **7**:1-17.
- [11] Gorban A.N., Zinovyev A.Y., Wunsch D.C. Application of The Method of Elastic Maps In Analysis of Genetic Texts. (2003) In *Proceedings of International Joint Conference on Neural Networks (IJCNN)*, Portland, Oregon, July 20-24.
- [12] Gorban A, Zinovyev A, Popova T. Seven clusters in genomic triplet distributions. (2003) *In Silico Biology*. **V.3**, 0039. (e-print: <http://xxx.lanl.gov/abs/cond-mat/0305681>)
- [13] Gorban A.N., Zinovyev A.Yu., Popova T.G. Statistical approaches to the automated gene identification without teacher // Institut des Hautes Etudes Scientifiques. - IHES Preprint, France. 2001. - M/01/34. Available at <http://www.ihes.fr> web-site.
- [14] Gorban A.N., Zinovyev A.Yu. Visualization of data by method of elastic maps and its applications in genomics, economics and sociology // Institut des Hautes Etudes Scientifiques. - IHES Preprint, France. 2001. - M/01/36. Available at <http://www.ihes.fr> web-site.
- [15] Karlin S. (1998) Global dinucleotide signatures and analysis of genomic heterogeneity. *Current opinion in microbiology* **1**(5): 598-610.
- [16] Lobry JR, Chessel D. (2003) Internal correspondence analysis of codon and amino-acid usage in thermophilic bacteria. *J.Appl.Genet.* **44**(2):235-61.
- [17] Mathe C., Sagot M.F., Schiex T., Rouze P. Current methods of gene prediction, their strengths and weaknesses (2002) *Nucleic Acids Res.* **30**(19):4103-4117.
- [18] Nicolas P, Bize L, Muri F, Hoebelke M, Rodolphe F, Ehrlich SD, Prum B, Bessieres P. Mining *Bacillus subtilis* chromosome heterogeneities using hidden Markov models. (2002) *Nucleic Acids Res.* **30**(6):1418-26.
- [19] Ou HY, Guo FB, Zhang CT. Analysis of nucleotide distribution in the genome of *Streptomyces coelicolor* A3(2) using the Z curve method. (2003) *FEBS Lett.* Apr 10; **540**(1-3):188-94.
- [20] Salzberg S.L., Delcher A.L., Kasif S., White O. Microbial gene identification using interpolated Markov Models. (1998) *Nuc. Acids Res.* **26**(2): 544-548.
- [21] Trifonov,E.N. Translation framing code and frame-monitoring mechanism as suggested by the analysis of mRNA and 16S rRNA nucleotide sequences. (1987) *J.Mol.Biol.* **194**,643-652.
- [22] Zhang,C.T.and Zhang,R. Analysis of distribution of bases in the coding sequences by a diagrammatic technique. (1991) *Nucleic Acids Res.* **19**,6313- 6317.
- [23] Zhang,C.T.and Chou,K.C. A graphic approach to analyzing codon usage in 1562 *Escherichia coli* protein coding sequences. (1994) *J.Mol.Biol.* **238**,1-8.
- [24] Zinovyev A. Visualizing the spatial structure of triplet distributions in genetic texts. - IHES Preprint, France. 2002. - M/02/28. Available at <http://www.ihes.fr> web-site.
- [25] Zinovyev A., Gorban A., Popova T. Self-Organizing Approach for Automated Gene Identification. (2003). *Open Systems and Information Dynamics* **10**(4). p.321-333.